A Parallel-type Load Damping Factor Controller for Frequency Regulation in Power Systems with High Penetration of Renewable Energy Sources

Zhe Zhang, Siyang Liao, *Member*, *IEEE*, Yuanzhang Sun, *Senior Member*, *IEEE*, Jian Xu, *Senior Member*, *IEEE*, Deping Ke, Bo Wang, Rui Chen, and Yibo Jiang

***Abstract*—Renewable energy sources (RESs) are rapidly developing and their substitution for traditional power generation poses significant challenges to the frequency regulation in power systems. The load damping factor *D* characterizes the active power of load that changes with power system frequency, which is an important factor influencing the frequency response. However, the value of *D* is small, resulting in the limitation in frequency regulation of the power system. This paper proposes a parallel-type load damping factor controller to enhance load damping factor by utilizing static var generators (SVGs) in substations. Additionally, it discusses the configuration method for the relevant parameters of the controller, evaluates its frequency regulation capability, investigates the impact of large-scale application of the controller on static and dynamic loads, and conducts a comprehensive evaluation of the impact of the damping factor control process on the voltage stability of the main grid. The large-scale application of the proposed controller can significantly improve the frequency regulation capability, and almost have no influence on the working status of the load. It can also significantly improve the dynamic performance of system frequency. The proposed controller can provide technical support for the frequency regulation of new power systems with high proportion of RESs.**

***Index Terms*—Load damping factor, parallel-type load damping factor controller, power system frequency regulation, high-proportion renewable energy system.**

I. Introduction

ONE of the basic conditions for power system stability is to consistently maintain the frequency stability [1]. With the proposal of various environmental protection policies [2] and the technological advancement of electronic devices, renewable energy sources (RESs) are gradually substituting traditional thermal power plants, which has posed great challenges to frequency regulation of power systems [3]. Meanwhile, the substitution of thermal power plants has reduced the capacity of traditional frequency regulation units and thus reduced their spinning reserves.

However, the fluctuations and stochastic characteristics of RESs make it more difficult to balance the power of generation and load [4]. When events such as power generation losses or direct current (DC) latch-up occurs, power systems with high proportions of RESs will experience greater frequency deviations.

The imbalance of generation and load leads to frequency deviation [5], which means frequency regulation can be implemented from both the power generation and load sides. Frequency regulation methods on the supply side encompass the implementation of fast-start and rapid-response power sources such as gas turbine units and energy storage systems. Additionally, facilitating the participation of RESs in frequency regulation involves employing control methods such as virtual damping and inertia. However, traditional frequency regulation for thermal power generation is expensive and environmental-unfriendly. The participation of RESs in frequency regulation technology is not yet technically mature, which requires expensive energy storage devices and inverters along with complex control systems, and will make the operating point of RES deviate from its maximum value, thereby reducing the efficiency of renewable generation [5]. Large-scale energy storage has not been widely applied due to economic and security reasons. Therefore, more and more scholars have begun to study the frequency regulation of the power system on the load side [3], [6]. Reference [6] firstly proposed the concept of demand-side management by controlling the switch status or power-related parameters of the load to involve it in frequency regulation. The National Grid Company in the UK and the Pacific Northwest National Laboratory in the USA have conducted projects on demand-side

Manuscript received: October 4, 2023; revised: October 26, 2023; accepted: November 28, 2023. Date of CrossCheck: November 28, 2023. Date of online publication: January 2, 2024.

This work was funded by the State Grid Corporation of China (No. SGJSSZ00KJS2310831) "Research and application of key technologies for load flexibility resource mining and power grid regulation driven by industrial Internet".

Z. Zhang, S. Liao (corresponding author), Y. Sun, J. Xu, D. Ke, and B. Wang are with the Hubei Engineering and Technology Research Center for AC/DC Intelligent Distribution Network, School of Electrical Engineering and Automation, Wuhan University, Wuhan 430072, China (e-mail: zhezhang@whu.edu.cn; liaosiyang@whu.edu.cn; yzsun@mail.tsinghua.edu.cn; xujian@whu.edu.cn; kedeping@whu.edu.cn; wangbo_eee@whu.edu.cn).

R. Chen is with the State Grid Hubei Electric Power Company Limited Economic Research Institute, Wuhan 430074, China (e-mail: rui-chen@whu.edu.cn).

Y. Jiang is with the State Grid (Suzhou) City & Energy Research Institute Company Limited, Suzhou 215000, China (e-mail: jiangyibo@whu.edu.cn).

DOI: 10.35833/MPCE.2023.000754

response. By signing agreements with users and installing smart devices, the potential of adjusting load power can be explored. Through aggregation, a large amount of load power can become a considerable resource for frequency regulation. However, the participation of massive users also mean that a large number of smart devices need to be installed, which will bring huge communication pressure, cumbersome workload, and users' privacy issues. Also, to ensure the users' good experience, the types of controllable loads are relatively limited, which mainly include temperature-sensitive loads and resistive loads [7].

Currently, there is a growing interest in load power regulation by adjusting the voltage of distribution network transformers. Reference [8] introduced the concept of "voltage-led load management", while [5] used a smart transformer (ST) to regulate feeder line voltage and control load power. More recently, [9] used electronic springs for feeder voltage control and consequent load power management. However, the previous works did not propose methodical theories or technical solutions to address the issue of load frequency regulation on a large scale. For instance, they did not consider the numerical quantification of load frequency regulation ability. Additionally, the impacts of equipment working in conjunction with power generators and the utilization of a large number of devices on the main grid and load were not analyzed. The range in which the large-scale application of load control can ensure the safety of the power system in different scenarios still remains unclear.

This paper proposes a parallel-type load damping factor controller to solve the above-mentioned problems, and improves the frequency stability by utilizing voltage control devices such as static voltage generators (SVGs) in substations to enhance the load damping factor. The proposed controller introduces a feedback control of system frequency deviation to substation load bus voltage, aiming to regulate the load power according to the system frequency deviation. The proposed controller is mainly characterized by two key features: load damping factor control and parallel-type. ① Load damping factor control: load damping factor is a natural characteristic of the load active power that changes with the system frequency, which indicates the percentage change of load active power when the system frequency changes by 1% [1]. Under natural conditions, the load damping factor is small and unchanged, which is around 1. By introducing the frequency deviation and voltage feedback control of substation load bus, the system frequency variation causes changes in load voltage, and the load active power also varies with the load voltage. Thus, the natural response of load active power to system frequency can be converted to controlled response and load. Theoretical calculations for the controlled load damping factor have been conducted in [10]: for the comprehensive load of a 10 kV feeder, the controlled load damping factors are distributed between 5 and 9; for electrolytic loads and thermal loads, the controlled load damping factor reaches an even higher value of 16.8, thereby greatly enhancing the numerical frequency-power response characteristic of the load and the frequency regulation ability in power system. ② Parallel-type: the controller needs to adjust the load bus voltage according to frequency deviation. Theoretically, this can be achieved by using a series-connected voltage regulator such as electronic fast adjustable voltage transformers or a parallel-type voltage regulator such as static var generator (SVG). This paper investigates a parallel-type load damping factor controller and chooses SVG as the voltage control equipment (series-connected devices can also be utilized; however, this paper does not conduct research on them). SVG can respond within 1 ms and completely solve the voltage control problems, especially when dealing with frequent load device start-ups [11]. In this paper, SVG is installed on the low-voltage side of the 110 kV/10 kV substation to transform the load into one with controllable damping factor characteristics.

The main contributions of this paper are described as follows. It presents a comprehensive theory and technology to address the issue of large-scale load participating in frequency control. A novel parallel-type load damping factor controller is proposed to enhance the load damping factor in power systems. This controller utilizes SVG installed on the low-voltage side of the 110 kV/10 kV substation and employs frequency deviation as the feedback signal to regulate the load bus voltage. The configuration method for the relevant parameters of the controller is discussed and verified through simulations. The frequency regulation ability of the controller is evaluated in value. The feasibility of widespread adoption of the proposed controller has been confirmed in power systems with high proportion of RESs. It enables the load to participate in frequency regulation tasks while remaining the voltage stability of the power system.

This paper is structured as follows. Section II introduces the methodology for designing the parallel-type load damping factor controller. Section III presents the simulation results and analysis. Finally, Section IV concludes this paper.

II. Methodology

A. Controlled Load Damping Factor and Load Modeling

Here, we firstly introduce the controlled load damping factor and then discuss the controlled load damping factor of composite load.

1) Controlled Load Damping Factor

The concept of controlled load damping factor was firstly proposed in [10]. For the readability of this paper, we will briefly introduce the concept and implementation methods of the controlled load damping factor.

Let us first review the conventional load damping factor, denoted by D, which is a natural characteristic of the load power changing with the system frequency, as shown in (1).

$$D = \frac{\Delta P_L^*}{\Delta f^*} \tag{1}$$

where Δf^* is the change of system frequency; and ΔP_L^* is the corresponding change value of load power change; and the superscript "*" represents the normalized value. Since D is a natural characteristic of load, it is defined as the natural load

damping factor in this paper.

Under natural conditions, D is small, which is around 1-1.5 [10]. The frequency-power response characteristic of the load β_L, which is relevant to D, is also small:

$$\beta_L = D\frac{P_L}{f_n} \tag{2}$$

where f_n is the rated frequency of the power system; and P_L is the rated load power.

In [10], a novel controlled load damping factor was proposed. The controlled load damping factor was conducted by introducing a load-voltage-frequency controller: when there is a generation loss or surplus in power system that causes frequency deviation Δf^*, the voltage of the overall load buses V_{Ll} (the subscript l denotes the index of load buses) can be controlled by introducing a feedback control amplification factor of voltage and frequency, denoted by K_{fvl}. Thus, the voltage variation of the overall load buses can be expressed as:

$$\Delta V_{Ll}^* = K_{fvl}\Delta f^* \quad l = 1, 2, ..., L_d \tag{3}$$

where L_d is the total number of load buses; and K_{fvl} is defined as frequency-voltage feedback coefficient.

When the bus voltage of the l^{th} composite load (supplied by a 110 kV/10 kV substation) changes by ΔV_{Ll}^*, the active power of the l^{th} composite load changes by ΔP_{Ll}^*, and the ratio between the two is defined as K_{Ll} [10]:

$$K_{Ll} = \frac{\Delta P_{Ll}^*}{\Delta V_{Ll}^*} \quad l = 1, 2, ..., L_d \tag{4}$$

According to the definition of the load damping factor in (1), the equation for the controlled load damping factor D_{cl} can be obtained by combining (3) and (4):

$$D_{cl} = \frac{\Delta P_{Ll}^*}{\Delta f^*} = \frac{\Delta V_{Ll}^*}{\Delta f^*}\frac{\Delta P_{Ll}^*}{\Delta V_{Ll}^*} = K_{fvl}K_{Ll} \quad l = 1, 2, ..., L_d \tag{5}$$

Theorem [10]: by introducing frequency-voltage feedback control in 10 kV bus, i.e., $\Delta V_{Ll}^* = K_{fvl}\Delta f^*$, the load damping factor is increased from its natural damping factor of D_l to $D_{cl} + D_l$.

2) Controlled Load Damping Factor of Composite Load

This paper mainly studies the characteristics of load under the 110 kV bus, i.e., composite load, assuming that the three types of loads (industrial, residential/commercial, and agricultural loads) are connected to the 110 kV bus via 110 kV/10 kV transformers. The derivation process of the controlled load damping factor of composite load will be presented in this part.

In this paper, the proportions of active power for industrial, residential/commercial, and agricultural loads under the 110 kV bus are denoted by p_{IL}, p_{RL}, and p_{AL}, respectively ($p_{IL} + p_{RL} + p_{AL} = 1$). Each type of load is connected to the 110 kV bus through a 110 kV/10 kV transformer.

The controlled load damping factor of the l^{th} composite load D_{cl} can be represented as the weighted average value of controlled damping factors for these three types of loads:

$$\begin{aligned} D_{cl} &= \frac{(\Delta P_{ILl} + \Delta P_{RLl} + \Delta P_{ALl})/P_{Ll0}}{\Delta f^*} = \\ &p_{IL}\frac{\Delta P_{ILl}}{P_{ILl0}\Delta f^*} + p_{RL}\frac{\Delta P_{RLl}}{P_{RLl0}\Delta f^*} + p_{AL}\frac{\Delta P_{ALl}}{P_{ALl0}\Delta f^*} = \\ &p_{IL}K_{fvILl}K_{ILl} + p_{RL}K_{fvRLl}K_{RLl} + p_{AL}K_{fvALl}K_{ALl} = \\ &p_{IL}D_{cILl} + p_{RL}D_{cRLl} + p_{AL}D_{cALl} \end{aligned} \tag{6}$$

where the subscripts *ILl*, *RLl*, and *ALl* represent the industrial load, residential/commercial load, and agricultural load belonging to the l^{th} composite load, respectively; ΔP is the load variation; subscript 0 represents the rated value; K_{ILl}, K_{ALl}, and K_{RLl} are the ratios of load active power change and load bus change for the three types of loads; and K_{fv} is the frequency-voltage feedback control parameter.

The value of load damping factor of composite load after frequency-voltage feedback control $D_{cl} + D_l$ can be derived from experimental data and by setting the value of frequency-voltage feedback control parameter. The value of natural load damping factor D_l is 1, which is given in [10]. Then, the value of controlled load damping factor D_{cl} is determined by three factors, as shown in (6): the proportions of three types of loads p_{IL}, p_{RL}, p_{AL}, the ratios of load active power change and load bus change K_{ILl}, K_{ALl}, K_{RLl}, and the frequency-voltage feedback control parameters K_{fvILl}, K_{fvRLl}, K_{fvALl}. Firstly, this paper assumes that the proportion of active power for industrial, residential/commercial, and agricultural loads under the 110 kV bus is 0.5: 0.4: 0.1. Secondly, the ratio between load active power change and voltage change can be derived from on-site experimental data [10] of three types of substations: industrial load areas, residential/commercial load areas, and agricultural load areas. The data include voltage disturbance data at substations and the corresponding power change data, and the ratio between these two can be derived. As for the feedback control parameter, its setting method will be discussed in the following text. The calculation process will also be elaborated.

B. Parallel-type Load Damping Factor Controller

1) Scheme of Load Damping Factor Controller

As shown in Fig. 1, the parallel-type load damping factor controller is implemented by SVG: the controller is connected in parallel to the 10 kV load feeder, and changes the load power by controlling the feeder voltage, so that the load has frequency control capability. The control structure consists of two parts. The red box shows the controlled load damping factor proposed in [10], which calculates the voltage reference value of SVG according to the controlled load damping factor. By introducing the frequency-voltage feedback coefficient K_{fv}, the corresponding bus voltage reference value is calculated according to the frequency deviation. The blue box shows the SVG control. After receiving the bus voltage reference value, SVG adjusts the bus voltage accordingly based on the bus voltage reference value and the active power reference value (set to be 0 in this paper). In Fig. 1, f is the system frequency; V_1 and V_L are the voltages at both sides of transformer; V_{ref} and P_{ref} are the reference voltage and power, respectively; I_{svg} and P_{svg} are the output current and power of the SVG, respectively; I_{dsvg} and I_{qsvg} are the *d*-

and q-components of I_{svg}, respectively; and i_{qref} is the q-component of the reference current. Furthermore, PI represents the proportional-integral controller; and PWM represents pulse width modulation.

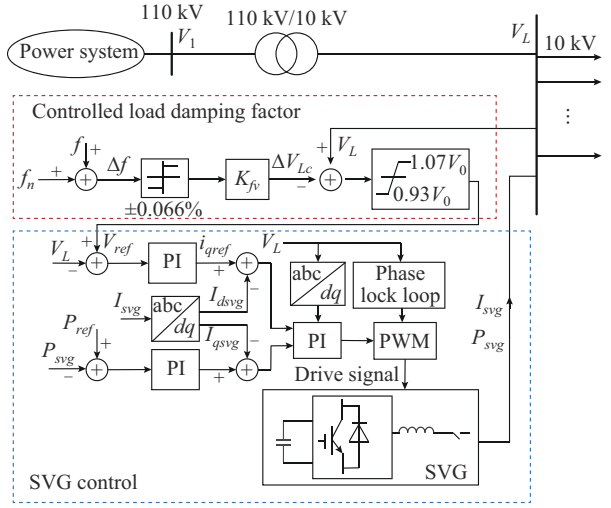

Fig. 1. Parallel-type load damping factor controller.

2) Setting of Frequency-voltage Feedback Coefficient K_{fv}

The main control parameter for the controller is the frequency-voltage feedback coefficient, and the principle of setting this coefficient is to ensure that the system operates safely while maximizing the adjusting potential of the load. Specifically, the following three requirements must be met.

1) The voltage at the bus where the load is located must be within the safe voltage range. According to current Chinese standards [12], for three-phase power supply of 20 kV and below, the limit for voltage deviation from the nominal value $\Delta V_{\max}$ is ±7%:

$$\Delta V_{\max} = \pm 7\% \tag{7}$$

2) The system frequency must be within the normal operating range. According to [13], the limit for system frequency deviation from the nominal value $\Delta f_{\max}$ is ±1%:

$$\Delta f_{\max} = 0.5/50 = 1\% \tag{8}$$

3) To maximize frequency regulation potential of the load, the frequency-voltage feedback coefficient for the load should be set to the maximum value allowed under the given conditions.

Therefore, the idea behind setting the frequency-voltage feedback coefficient is to assume that the voltage deviation of the load reaches its maximum value when the frequency deviation is at its maximum [10]:

$$K_{fv} = \frac{\Delta V_{L,\max}}{\Delta f_{\max}} \tag{9}$$

$$\Delta V_{L,\max} = \begin{cases} 1.07 - V_{LS} & \Delta f \geq 0.5 \text{ Hz} \\ V_{LS} - 0.93 & \Delta f \leq -0.5 \text{ Hz} \end{cases} \tag{10}$$

where V_{LS} is the steady-state operating point of the load voltage under normal conditions.

Under steady-state operating conditions, the load needs to have both upward and downward regulation capabilities. However, the values of the upward and downward regulation power are mutually exclusive, and an increase in the upward regulation capability of the load will inevitably lead to a decrease in its downward regulation capability. In order to make the upward and downward regulation capacities of the load equal, the load bus voltage is adjusted to a more appropriate value of 1 p.u.. The corresponding frequency-voltage feedback coefficient for the controller is:

$$K_{fv} = \frac{7\%}{1\%} = 7 \tag{11}$$

3) Setting of SVG Capacity

In order to control the load bus voltage with SVG, it is necessary for SVG to have a sufficiently large control capacity. However, considering the economic feasibility of the equipment, the SVG capacity cannot be too large. Therefore, it is necessary to set an appropriate SVG capacity. The theoretical analysis and actual calculation results of SVG capacity are shown below.

1) Theoretical analysis on setting of SVG capacity

Firstly, the external power grid of the controlled load is equivalently processed into the form of a voltage source in series with an impedance. The parameters of the voltage source and reactance are obtained through identification, and this paper adopts the identification method proposed in [14]. Before and after the installation of SVG, the equivalent model structures are shown in Fig. 2.

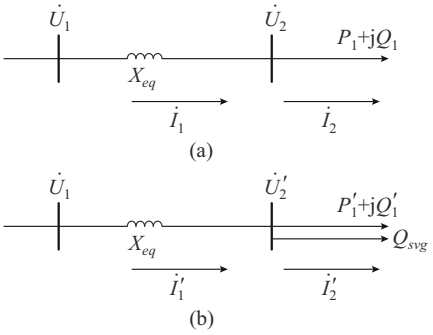

Fig. 2. Equivalent model structures. (a) Before installation of SVG. (b) After installation of SVG.

As shown in Fig. 2(a), the currents at both ends of the load bus, i.e., $\dot{I}_1$ and $\dot{I}_2$, are equal:

$$\dot{I}_1 = \dot{I}_2 \tag{12}$$

Based on (12), before the installation of SVG, it can be derived that:

$$\frac{\dot{U}_1 - \dot{U}_2}{jX_{eq}} = \frac{P_1 - jQ_1}{\dot{U}_2} \tag{13}$$

where X_{eq} is the reactance of the transformer; P_1 and Q_1 are the active and the reactive power of the load, respectively; and $\dot{U}_1$ and $\dot{U}_2$ are the voltages of the 110 kV bus and the 10 kV bus, respectively.

After installation of SVG, it can be derived that:

$$\frac{\dot{U}_1 - \dot{U}_2'}{jX_{eq}} = \frac{P_1' - j(Q_1' + Q_{svg})}{\dot{U}_2'} \tag{14}$$

where $\dot{U}_2'$ is the load voltage after control; and Q_{svg} is the reactive power output by SVG. And $\dot{I}_1'$ and $\dot{I}_2'$ are the currents at both ends of the load bus after installation of SVG.

The value of $\dot{U}_1$ can be derived as:

$$\dot{U}_1 = \mathrm{j}X_{eq}\frac{P_1 - \mathrm{j}Q_1}{\dot{U}_2} + \dot{U}_2 \tag{15}$$

The capacity of the reactive power compensation device is determined by solving (14) and (15) simultaneously:

$$Q_{svg} = -\mathrm{Im}\left(\frac{\dot{U}_1 - \dot{U}_2'}{\mathrm{j}X_{eq}}\dot{U}_2'\right) - Q_1' \tag{16}$$

2) Results of setting of SVG capacity

We first utilize the Thevenin equivalent circuit to illustrate the variation pattern of SVG output with changes in load power factor and controlled voltage. Based on this pattern, the operating point at which the SVG output is maximized can be calculated, representing the optimal SVG capacity. Subsequently, the SVG capacity installed at each load node can be computed in an actual power system.

First, taking a single-machine power system as an example, when designing the SVG capacity, it is necessary to consider the allowable voltage adjustment range of the bus voltage and the capacity of the substation. The SVG capacity increases with a larger voltage regulation range and substation capacity. The national standard allows a 7% adjustment for bus voltages below 10 kV, and each 110 kV/10 kV substation has a maximum power supply of 50 MW. The specific calculation results for the SVG capacity are as follows.

The reactive power output of SVG is calculated and simulated under the following conditions: ① different load power factors; ② different controlled voltages of the 10 kV bus. The results are shown in Figs. 3 and 4, where a negative sign represents compensating capacitive reactive power.

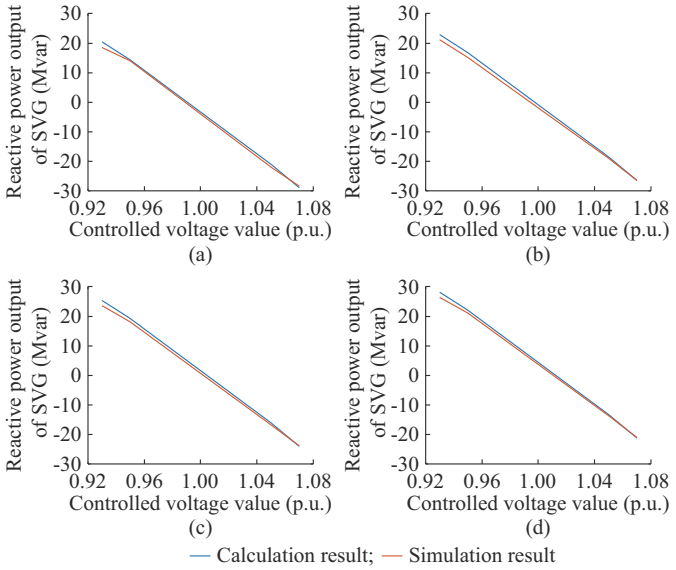

Fig. 3. Reactive power output of SVG under different power factors. (a) Power factor is 0.9. (b) Power factor is 0.92. (c) Power factor is 0.94. (d) Power factor is 0.96.

From Figs. 3 and 4, it can be observed that the simulation results are very close to the calculation results, which verifies the accuracy of the calculation results. The specific capacity of the SVG is related to the value of X_{eq} in the equivalent model.

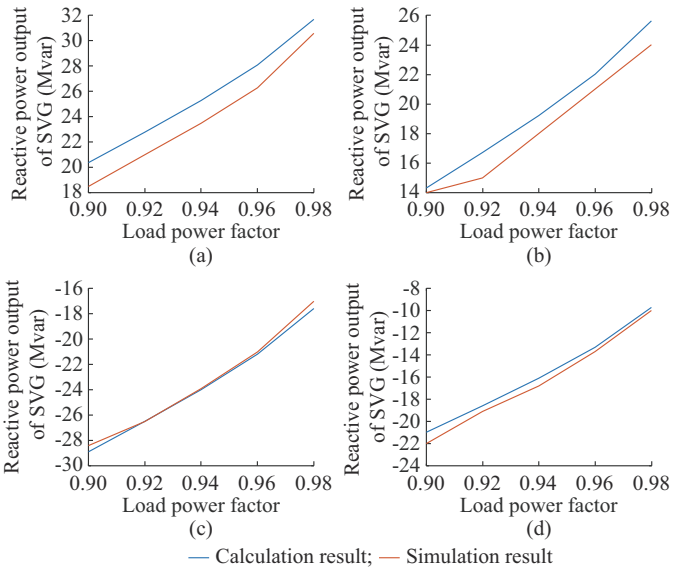

Fig. 4. Reactive power output of SVG under different controlled voltages. (a) Controlled voltage value is 0.93 p.u.. (b) Controlled voltage value is 0.95 p.u.. (c) Controlled voltage value is 1.05 p.u.. (d) Controlled voltage value is 1.07 p.u..

The reactive power output of SVG decreases as the controlled voltage increases. When the voltage decreases, the SVG compensates for more inductive reactive power, resulting in a lower voltage drop. When the voltage increases, the SVG compensates for more capacitive reactive power, resulting in a higher voltage increase.

The active power output of SVG increases with the load power factor. When the voltage decreases, the larger the load power factor, the more inductive reactive power needs to be compensated during voltage regulation. When the voltage increases, the larger the load power factor, the less capacitive reactive power needs to be compensated during voltage regulation.

The SVG is installed on the low-voltage side of the 110 kV/10 kV substation to regulate the 10 kV bus voltage. There are a total of 9 substations in the region, and the power factor of the load under each substation is 0.92. The SVG output reaches its maximum capacitive and reactive power outputs when the controlled voltage reaches the upper and lower limits, i.e., 0.93 p.u. and 1.07 p.u., respectively. In an actual power system, the specific SVG capacity is related to the value of X_{eq} in the equivalent model. In the actual Yunnan power grid in China, due to the large amount of loads, the aggregated load model is used, and the SVG capacity is expressed as the proportion of its actual capacity to the capacity of the 110 kV/10 kV equivalent transformer, as shown in Table I. The final SVG capacity is the capacitive reactive power with a larger value, and the range of the SVG capacity is from 16.4% to 25.1% of the transformer capacity.

III. Simulation Results and Analysis

Simulation studies are conducted based on the actual Yunnan power grid in China. Generation loss and surplus faults have taken place in the system, and the behaviors of the power system with and without the parallel-type load damping factor controller are compared.

TABLE I
PROPORTION OF SVG CAPACITY TO TRANSFORMER CAPACITY

Transformer	Inductive reactive power (%)	Capacitive reactive power (%)	Transformer	Inductive reactive power (%)	Capacitive reactive power (%)
1	18.8	25.1	6	10.8	16.4
2	19.4	23.6	7	12.5	18.4
3	19.0	24.9	8	11.9	18.8
4	18.8	24.7	9	18.0	23.8
5	12.5	17.7			

This paper first studies a static load model. To further consider the control impact on motor loads, a dynamic load model is also studied.

A. System Model

1) Composition of Generation Load and Power

Assume that the power system is operating with abundant water supply where the hydropower is at full capacity, and the thermal power is responsible for frequency regulation. The spinning reserve spreads uniformly over thermal power generation. The speed regulation is $R=5\%$ for thermal generators. The natural load damping factor is $D=1$. Table II shows the composition of the generation power and load in the system.

TABLE II
COMPOSITION OF GENERATION POWER AND LOAD

Total load (MW)	Total installed capacity (MVA)	Installed hydropower capacity (MVA)	Installed thermal power capacity (MVA)	Reserve capacity distributed among thermal power units (MW)
27880	32800	4920	27880	8200

2) System Topology

Figure 5 shows the equivalent main topology of Yunnan power grid in China, where the internal power grid of Wenshan area is at the right-hand side of the red dotted line, and the external power grid is at the left-hand side.

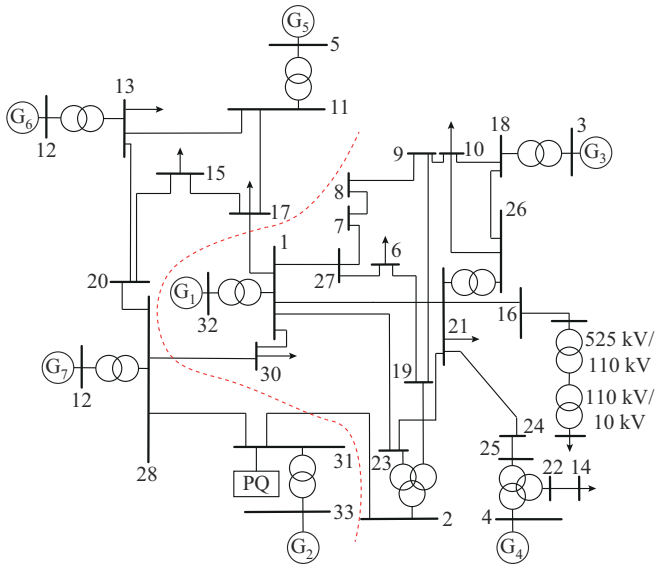

Fig. 5. Equivalent main topology of Yunnan power grid in China.

The load is connected to the main grid via 525 kV/110 kV or 230 kV/110 kV transformers, and 110 kV/10 kV transformers. In the topology, the transformer between the 10 kV feeder and the high-voltage bus is omitted, and only the simplified equivalent load is used to represent it. A parallel-type load damping factor controller is installed at each 110 kV/10 kV substation.

3) Load Model

1) Static load model

This paper mainly studies the characteristics of composite load under the 110 kV bus, assuming that the load is connected to the 110 kV bus via a 110 kV/10 kV transformer. The proportion of active power for industrial, residential/commercial, and agricultural loads under the 110 kV bus is 0.5:0.4:0.1. With reference to the measured data of the substations, exponential static characteristic models of three typical loads are built.

A static load model expresses the characteristics of the load at any time instant as algebraic functions of the bus voltage magnitude and system frequency. The active power of the load can be described precisely by an exponent model, as shown in (17), in which the exponential parameter α and the scale factor K_{pl} can be regarded as unchanged:

$$P_{Ll}=P_{Ll0}\left(\frac{V_{SLl}}{V_{Ll0}}\right)^{\alpha}\left(1+K_{pl}\frac{f-f_0}{f_0}\right)\quad l=1,2,...,L_d \tag{17}$$

where P_{Ll} is the active power component of the l^{th} load when the bus voltage is V_{SLl}; α is the voltage-active power factor of the load; and P_{Ll0}, V_{Ll0}, and f_0 are the values at the initial operating point for P_{Ll}, V_{Ll}, and f, respectively.

Similarly, the reactive part of the load is represented as:

$$Q_{Ll}=Q_{Ll0}\left(\frac{V_{SLl}}{V_{Ll0}}\right)^{\beta}\left(1+K_{ql}\frac{f-f_0}{f_0}\right)\quad l=1,2,...,L_d \tag{18}$$

where Q_{Ll} is the reactive power component of the l^{th} load when the bus voltage is V_{SLl} and the system frequency is f; β is the exponential parameter; K_{ql} is the scale factor; and Q_{Ll0} is the value at the initial operating point for Q_{Ll}.

The parameters in the static load model of active power can be obtained through theoretical analysis and experimental data, and the model parameters are related to the controlled damping factor: [10] proves that the frequency-active power coefficient K_{pl} in the static load model has the same value as the natural load damping constant D. Both of their values can be obtained through dividing the change in load active power by the change in system frequency:

$$D=K_{pl}=\frac{\Delta P_{Ll}}{\Delta f} \tag{19}$$

The voltage-active power factor of the load α can be obtained through linearization:

$$\frac{P_{Ll}}{P_{Ll0}}=\left(\frac{V_{Ll0}+\Delta V_{Ll}}{V_{Ll0}}\right)^{\alpha}\left(1+K_{pl}\frac{\Delta f}{f_0}\right)=\left(1+\frac{\Delta V_{Ll}}{V_{Ll0}}\right)^{\alpha}\left(1+K_{pl}\frac{\Delta f}{f_0}\right)=\left(1+\alpha\frac{\Delta V_{Ll}}{V_{Ll0}}\right)\left(1+K_{pl}\frac{\Delta f}{f_0}\right) \tag{20}$$

Compared with (4), it can be observed that the power exponent coefficient α in the static load model has the same

numerical value:

$$\frac{\Delta P_{Ll}}{\Delta V_{Ll}} = \alpha = K_{Ll} \tag{21}$$

By combining (6) and (21), we can derive an expression for the controlled load damping factor as:

$$D_{cl} = (p_{ILl}\alpha_{IL} + p_{RLl}\alpha_{RL} + p_{ALl}\alpha_{AL})K_{fv} \tag{22}$$

where p is the proportion of each kind of load. Reference [10] provides on-site experimental data from three types of substations: industrial, residential/commercial, and agricultural load areas, including voltage disturbance data at substations and the corresponding power change data. Using the experimental data [10], the exponential coefficients of different load models can be obtained, as shown in Table III. Also, according to (22), the controlled load damping factor is calculated to be 6.3. The load damping factor is then increased to 7.3. The other parameters of the load model can be referred from [15].

TABLE III
EXPONENTIAL COEFFICIENTS OF DIFFERENT LOAD MODELS

Load type	α
Industrial load	0.7
Residential/commercial load	1.0
Agricultural load	1.5

2) Dynamic load model

The static load model can reflect the system frequency in steady state, but in practical situations, there are a large number of motor loads in the power system. In order to evaluate the impact of controller-induced voltage changes on load behaviors, a dynamic load model is also established in this paper.

According to the data provided by the Load Model Research Group of the State Grid Corporation of China, the load models used by the dispatch departments in various regions of China are mostly constant impedance models and motor models combined in a certain proportion [16]. The proportion of motor models ranges from 40% to 65%. Therefore, in this paper, 40% of the static load is replaced by motor loads with the same active power. The model and parameters of the motor load are based on the type-6 typical induction motor data recommended by the IEEE Task Force on Load Representation for Dynamic Performance [17].

B. Case 1: System Response to Generation Loss

In case 1, generation loss occurs in the power systems with and without parallel-type load damping factor controller. The purpose of case 1 is to study the frequency regulation ability of the controller, and its impact on the load working status and the main grid voltage when the system frequency reaches the lowest limit. At this point, the load can provide its maximum upward frequency adjustment capacity. Also, it is necessary to consider the extent to which motor loads and main grid voltage are affected under this extreme condition.

Cases 1.1 and 1.2 employ a static load model in the simulation to compare the theoretical calculation results with the simulation results; while cases 1.3 and 1.4 adopt a dynamic load model to investigate the influence of the controller on the motor load. In cases 1.1 and 1.3, the power generation loss causes the frequency of the normal system to decrease to its lowest limit and the same generation loss happens in the system with load damping factor controller. In cases 1.2 and 1.4, the frequency of the system with load damping factor controller reaches its lowest limit. At last, the impact of controller voltage regulation on the main grid voltage is evaluated.

1) Control Effect of Controller and Its Impact on Different Loads

1) Case 1.1

Case 1.1 adopts a static load model and compares between the systems with and without the load damping factor controller under a generation loss situation.

First, theoretical calculations are carried out. Assume that the generation units without frequency regulation ability lose power generation, resulting in system frequency as low as 49.5 Hz in the normal system. The power generation loss in the uncontrolled system is given as [10]: $\Delta P = (P_L D_l + P_G/R) \times 0.5 = 1918.8$ MW, where D_l is the natural load damping; and P_G is the total active power of the generator.

When the same power generation loss happens in the controlled system, the calculation result for the steady-state frequency is $\Delta f_{DC} = \Delta P / \{[P_G/R + P_L(D_{cl} + D_l)]/50\} = 0.26$ Hz, where $P_G/R = 3280$ MW/Hz, $P_L D_l = 557.6$ MW/Hz, and $P_L(D_{cl} + D_l) = 4070.48$ MW/Hz.

The RTDS simulation results in Fig. 6 are similar to the theoretical calculation results, with errors caused by transmission power losses. Due to the load damping factor controller, the steady-state frequency deviation of the system can be reduced to half of the system without the controller. It is noted that different colors of curves in Fig. 6(d)-(e) represent different loads.

Figure 7 shows the static frequency characteristics of load and generator in case 1.1, which is a graphical explanation of the principle of the load damping factor. As shown in the static frequency characteristic curves of the load and the generator in Fig. 7, the blue line represents the static frequency characteristic curve of the load, where P_{LD} represents the natural damping characteristic of the load; P_{LC} represents the controlled damping characteristic of the load, with a steeper slope; and f_{LN} and f_{LD} are the steady-state frequencies after disturbance of the normal system and controlled system, respectively. The red lines P_{G1} and P_{G2} are the power change curves of the generator before and after the disturbance, respectively. The two lines with black arrows in the figure show the power generation losses with the same length, meaning the same value. The red dashed line represents the increase in power output caused by the frequency regulation of the generator, while the blue dashed line represents the decrease in power consumption caused by the damping effect of the load. It can be clearly observed that under the same disturbance of reduced power generation, the steady-state frequency deviation of the system with load damping factor controller is smaller, and the load provides more adjustable power. Therefore, the amount of power that the generator needs to output for frequency regulation is reduced, which can greatly reduce the spinning reserve.

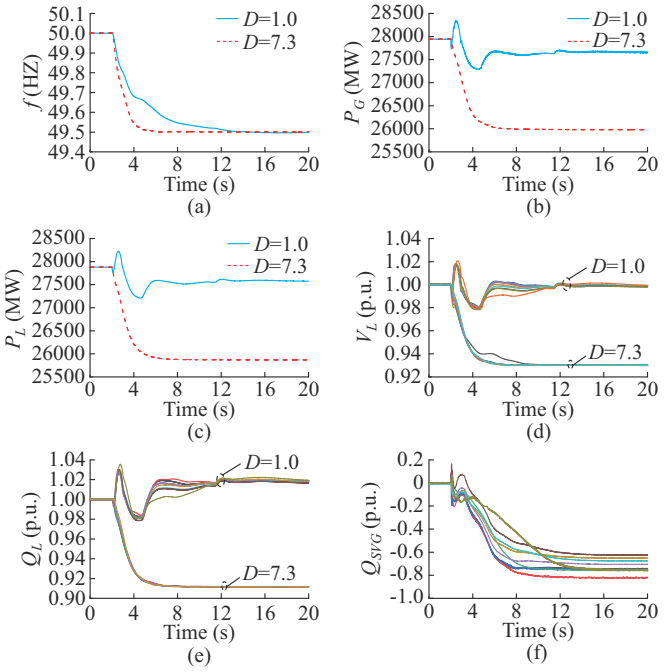

Fig. 6. Simulation results in case 1.1. (a) System frequency f. (b) Total active power of generator P_G. (c) Total load active power P_L. (d) Voltage of each load node V_L. (e) Reactive power of each load Q_L. (f) Output of each SVG Q_{svg}.

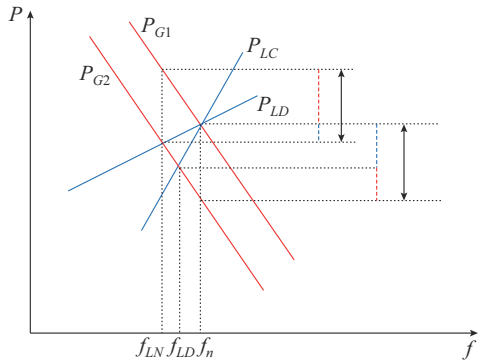

Fig. 7. Static frequency characteristics of load and generator in case 1.1.

The theoretical explanation in Fig. 7 can also be confirmed in Fig. 6. The power generation loss of 1926 MW is balanced by the decrease in load power and the increase in generator output power. The system with load damping factor controller provides 1070 MW regulation power, while the system without load damping controller can only provide 293 MW. Therefore, the frequency regulation burden of the generator units is much less in the system with load damping factor controller.

From the reactive power curves and voltage curves in Fig. 6, it can be observed that the rapid response of the controller can enable the load voltage to smoothly and quickly reach the set value.

2) Case 1.2

Adopting a static load model, the frequency of the system with load damping factor controller drops to 49.5 Hz.

Figure 8 shows the simulation results of both systems reaching the frequency limit of 49.5 Hz. The systems with and without load damping factor controller lose 3591 MW and 1926 MW of generation, respectively, which means the controlled load provide an additional 1665 MW of spinning reserve.

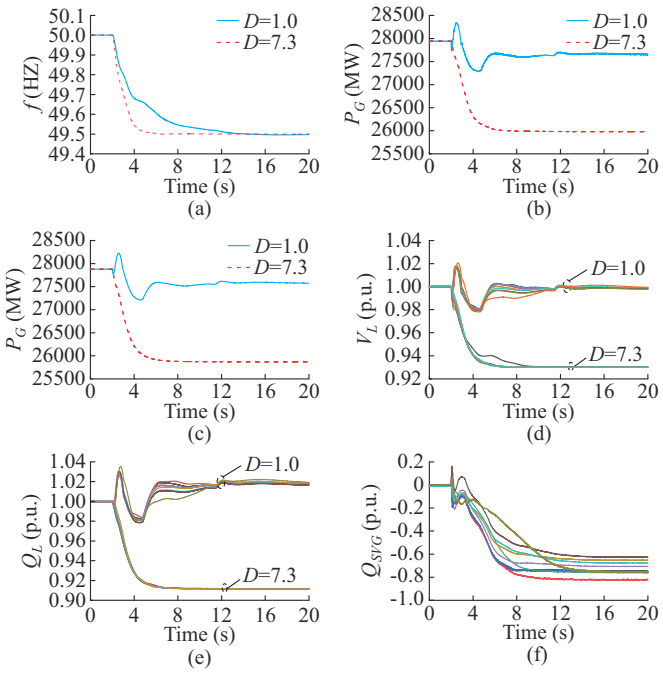

Fig. 8. Simulation results in case 1.2. (a) System frequency f. (b) Total active power of generator P_G. (c) Total load active power P_L. (d) Voltage of each load node V_L. (e) Reactive power of each load Q_L. (f) Output of each SVG Q_{svg}.

The theoretical equation for calculating the additional rotational reserve provided by the controlled damping factor load is:

$$\Delta P_{SR}=[P_L^2(D_{cl}+D_l)+P_G/R]\times 0.5-(P_L D_l+P_G/R)\times 0.5= D_{cl}P_L\times 0.5=1756.2\ \text{MW} \quad (23)$$

The theoretical calculation results are similar to the simulation results, and it can be observed from (23) that the equivalent spinning reserve is positively correlated with the value of controlled damping factor.

In Fig. 8(d), the voltage of the load feeder also reaches the minimum allowable value of 0.93 p.u. when the frequency is reduced to its limit, but due to the effect of voltage limit control, the voltage will always remain within the allowable range and will not exceed the limit.

3) Case 1.3

Case 1.3 adopts a comprehensive dynamic load model, and compares between the systems with and without load damping factor controller under a power generation loss.

In order to evaluate the frequency regulation ability and the impact of controllers in reducing the load voltage on the working performance of motor loads, a system model including motor loads is also established. The proportions of motor load and static load are 40% and 60%, respectively.

Figure 9 shows the simulation results of case 1.3. The load damping factor controller still has a good control effect on the comprehensive dynamic load, and the frequency control ability of the comprehensive dynamic load is much better than that of the system without load damping factor controller.

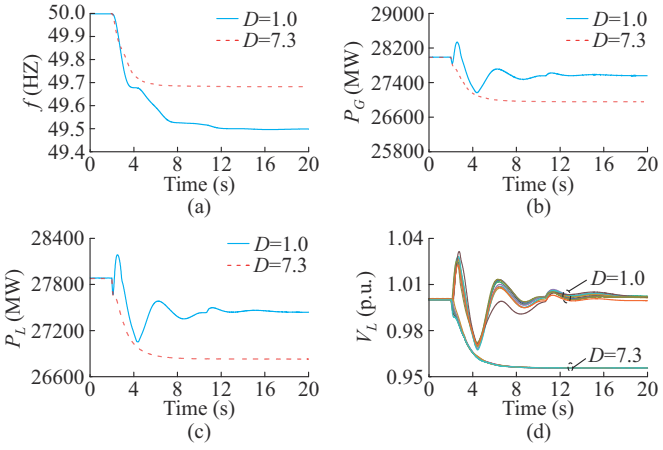

Fig. 9. Simulation results in case 1.3. (a) System frequency f. (b) Total active power of generator P_G. (c) Total load active power P_L. (d) Voltage of each load node V_L.

Figure 10 shows the comparison results in case 1.3, including the active and reactive power, as well as the electric motor torque of the static load and electric motor load. It can be observed that in the system with load damping factor controller, the dynamic process of the electric motor torque is smoother, and the steady-state values of the electromagnetic torque in both systems are basically the same, indicating that the performance of the electric motor has been improved with the controller.

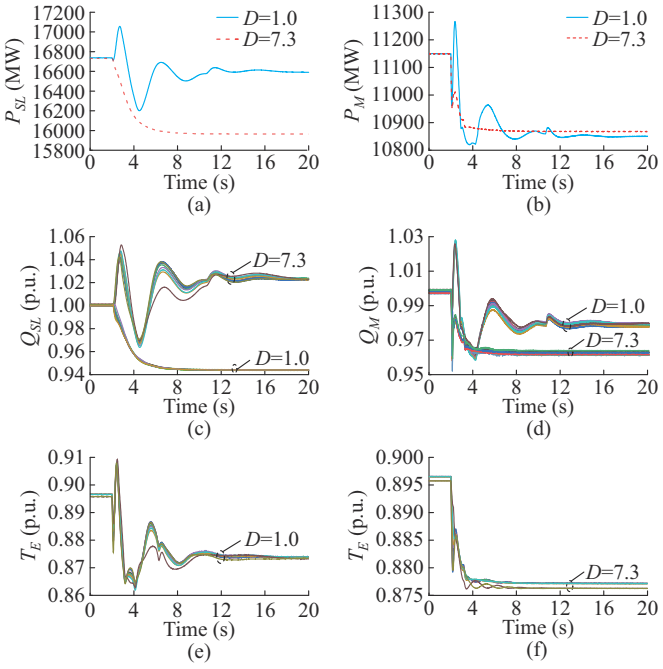

Fig. 10. Comparison results in case 1.3. (a) Total active power of static load P_{SL}. (b) Total active power of motor load P_M. (c) Reactive power of each static load Q_{SL}. (d) Reactive power of each motor load Q_M. (e) Electric motor torque T_E of each motor load without load damping factor controller. (f) Electric motor torque T_E of each motor load with load damping factor controller.

4) Case 1.4

Case 1.4 adopts a comprehensive dynamic load model while the frequency of the system with load damping factor controller drops to 49.5 Hz.

As shown in Fig. 11, a 3240 MW power generation loss causes the system frequency to drop to 49.5 Hz. Compared with the system without load damping factor controller in case 1.3, the system with load damping factor controller provides an additional 1175 MW spinning reserve. However, the extra spinning reserve supplied by the controlled damping factor is less than that of the static load model in case 1.2. This is because the active power of the motor load is not very sensitive to voltage change, so the load damping factor controller does not have as significant control effect as the static load model. However, there is still great room for improvement in load participating in frequency regulation. In the areas where the proportion of motor load is high, accurate modeling of the load should be performed, and the voltage-active power coefficient of the comprehensive load should be considered when setting the value of K_{fv}.

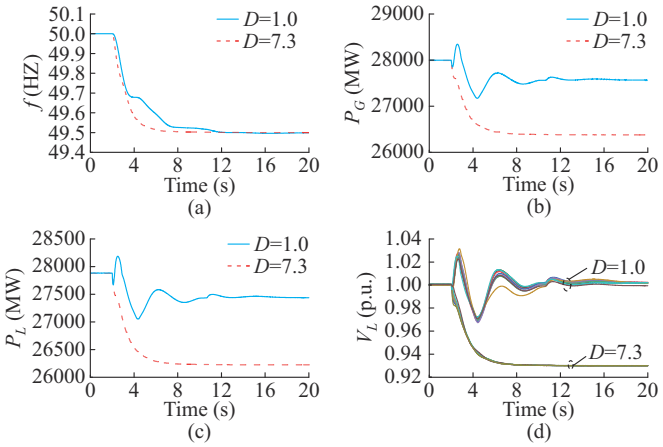

Fig. 11. Simulation results in case 1.4. (a) System frequency f. (b) Total active power of generator P_G. (c) Total load active power P_L. (d) Voltage of each load node V_L.

The curves of active and reactive power for static and dynamic loads in Fig. 12 also exhibit a similar pattern to those in case 1.3.

Comparing the electromagnetic torque of the generator in Fig. 12 and Fig. 10, it can be observed in Case 1.3 that the frequency reduction causes a 2.2% decrease in the electromagnetic torque while the combined effect of voltage and frequency reductions leads to a 3.4% decrease. This suggests that the impact of voltage decrease on the electric motor torque is negligible, further indicating that the load damping factor controller has a negligible effect on the operating conditions of the motor. In the controlled system, the dynamic process of the electric motor torque is smoother, and the steady-state values of the electromagnetic torque in both systems are basically the same, which means that the load damping factor controller can improve the dynamic performance of the motor.

The results of cases 1.1-1.4 and the above theoretical analysis indicate the following conclusions.

1) Under the same disturbance, the load damping factor controller can greatly reduce the steady-state frequency deviation of the system.

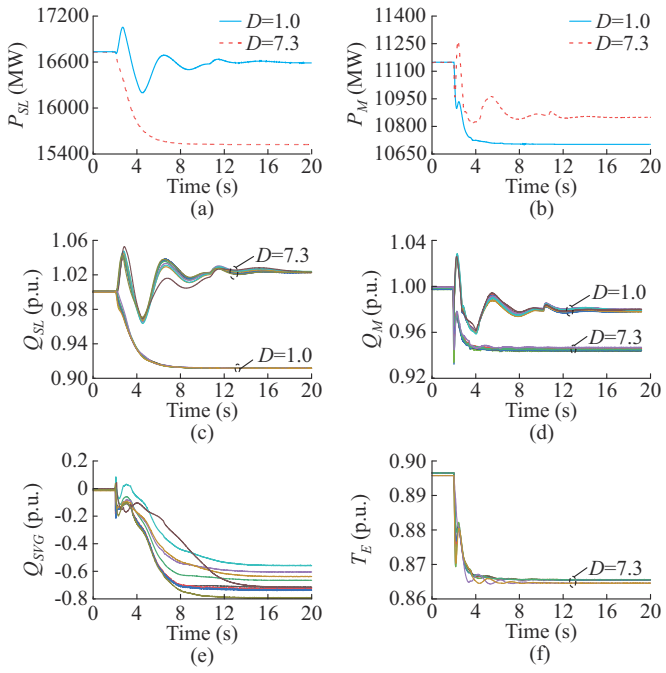

Fig. 12. Partial comparison results in case 1.4. (a) Total active power of static load P_{SL}. (b) Total active power of motor load P_M. (c) Reactive power of each static load Q_{SL}. (d) Reactive power of each motor load Q_M. (e) Output of each SVG Q_{SVG}. (f) Electric motor torque T_E of each motor load in system with load damping factor controller.

2) Controlled loads can provide a large amount of spinning reserve for the system (1665 MW in the system with static load and 1175 MW in the system with dynamic load).

3) Parallel-type load damping factor controllers can also improve the dynamic stability of the voltage and the performance of the motor.

2) Assessment of Impact of Controller Voltage Regulation on Main Grid Voltage

To reduce the voltage of the load feeder, SVG needs to absorb reactive power. After a large number of SVGs participate in the control, their impact on the main grid voltage should also be considered. The steady-state main grid voltages before and after power generation loss are shown in Table IV.

TABLE IV
STEADY-STATE MAIN GRID VOLTAGES BEFORE AND AFTER POWER GENERATION LOSS

Case	Range of main grid voltage before generation loss (p.u.)	Range of main grid voltage after power generation loss (p.u.)	
		With load damping factor controller	Without load damping factor controller
1.1	1.037-1.051	1.036-1.051	1.024-1.037
1.2	1.037-1.054		1.000-1.035
1.3	1.036-1.051	1.036-1.050	1.030-1.045
1.4	1.036-1.051		1.000-1.041

The simulation results show that the main grid voltage in the system with load damping factor controller is affected by the SVGs that absorb reactive power, but is still within the allowable range (0.93-1.07 p.u.).

C. Case 2: Response to DC System Fault

The actual Yunnan power grid in China operates as a terminus for DC transmission. In the scenarios where a blocking fault occurs, power generation cannot be exported, resulting in surplus generation power and an increase in system frequency. Similar to the case of power loss in case A, this sub-section investigates the steady-state frequency of the system when both of the systems experience the same power loss during power generation, as well as the situation where the frequency of the system with load damping factor controller reaches the highest limit. Furthermore, it shows the results of main grid voltage in both systems. Due to the similarity of the simulation results with case A, the summary of the simulation results in this subsection is presented in Table V and Table VI. Since the load regulation capability and generator frequency control remain unchanged, the experimental results exhibit symmetric characteristics compared with the case of reduced generation. The main grid voltage with load damping factor controller still does not exceed the limit.

TABLE V
STEADY-STATE FREQUENCY UNDER POWER SURPLUS CONDITION

Load type	Surplus generation power (MW)	Steady-state frequency deviation after disturbance (Hz)	
		With load damping factor controller	Without load damping factor controller
Static load	1935	0.26	0.5
	3675	0.50	
Dynamic load	2075	0.31	0.5
	3340	0.50	

TABLE VI
STEADY-STATE MAIN GRID VOLTAGE BEFORE AND AFTER POWER GENERATION INCREASE

Case	Range of main grid voltage before generation increase (p.u.)	Range of main grid voltage after power generation increase (p.u.)	
		With load damping factor controller	Without load damping factor controller
2.1	1.037-1.051	1.036-1.051	1.048-1.065
2.2	1.037-1.051		1.062-1.080
2.3	1.036-1.051	1.036-1.050	1.048-1.058
2.4	1.036-1.051		1.053-1.073

D. Effect of Load Damping Factor Controller in Power Systems with High Penetration Rate of RESs

This subsection studies the effect of load damping factor controller in power systems with high penetration rate of RESs. Assuming a gradual replacement of thermal power units in the system with RESs, when the penetration rate of RESs is 30%, the spinning reserve of the system is set to be 50% of the original system. Further, when the penetration rate reaches 60%, it is assumed that there is no spinning reserve in the system. The systems with and without load damping factor controller are studied under the same power generation loss and the same frequency deviation, and the effects of the load damping factor controller are evaluated from the perspectives of the equivalent spinning reserve pro-

vided by the controlled load and the steady-state frequency deviation of the system.

The simulation results with different penetration rates of RESs are shown in Table VII. As the penetration level of RESs increases, the allowed power generation deficit of the system becomes smaller and smaller. However, after applying the load damping factor controller, the allowed renewable generation fluctuation increases from 293.2 MW to 1991 MW and from 437.5 MW to 1637 MW, equivalent to controller providing up to an additional 1697.8 MW and 1199 MW of spinning reserve, respectively.

TABLE VII
SIMULATION RESULTS WITH DIFFERENT PENETRATION RATES OF RESS

Penetration rate of RESs (%)	Static load model				Dynamic load model			
	ΔP_1 without controller when frequency deviation is 0.5 Hz (MW)	Frequency deviation with controller when generation loss is ΔP_1 (Hz)	ΔP_2 with controller when frequency deviation is 0.5 Hz (MW)	Additional spinning reserve provided by load controllers (MW)	ΔP_3 without controller when frequency deviation is 0.5 Hz (MW)	Frequency deviation with controller when generation loss is ΔP_3 (Hz)	ΔP_4 with controller when frequency deviation is 0.5 Hz (MW)	Additional spinning reserve provided by load controllers (MW)
0	1926.0	0.2700	3591	1665.0	2065.0	0.32	3240	1175
30	1105.0	0.2000	2772	1667.0	1246.0	0.23	2417	1171
60	293.2	0.0726	1991	1697.8	437.5	0.13	1637	1199

Under the same disturbance, the frequency deviation of the system with load damping factor controller is smaller than that of the system without the controller. In the case of 60% penetration rate of RESs, when the frequency deviation of the system without the controller is 0.5 Hz, the frequency deviation of the system with the controller under the same disturbance is only 0.0726 Hz (with static load model) and 0.13 Hz (with dynamic load model), respectively. This indicates that the load damping controller can provide reliable frequency support for the system with high penetration rate of RESs, and reduce the steady-state frequency deviation.

The above two points illustrate that after applying load damping factor controller, a larger range of renewable energy fluctuations is allowed, and the load damping factor controller is beneficial for the high penetration of RESs into the system.

IV. CONCLUSION

This paper has proposed a novel parallel-type load damping factor controller to enhance the load damping factor by utilizing voltage control devices in substations. SVG is installed on the low-voltage side of the 110 kV/10 kV substation, and frequency deviation is used as a feedback signal for controlling the load bus voltage. The configuration method for the relevant parameters of the controller is discussed; the frequency regulation ability of the controller is evaluated; and the impact on static and dynamic loads and the main grid voltage are evaluated.

Simulation results indicate that with load damping factor controller, the steady-state frequency deviation of the system can be significantly diminished, offering increased spinning reserves. The equivalent spinning reserve is positively correlated with the value of the controlled damping factor. Furthermore, the controller does not affect the operational state of the load or the safety of the grid, and even improves the dynamic behavior of system voltage and motor loads.

More importantly, the load damping factor controller can greatly improve the frequency regulation capability of system with high penetration rate of RESs, reducing steady-state frequency deviation and providing reliable frequency support for such system.

This paper proposes both theories and technical solutions to address the issue of load frequency regulation on a large scale, which is beneficial to the integration of RESs into the system.

It is important to note that this paper does not account for the positive or negative interactions among multiple SVGs with the provided controller. This aspect will be addressed in future research endeavors. In addition, the current focus on active power generation fluctuations will be expanded to encompass inertia and damping terms in both theoretical and simulation studies.

REFERENCES

[1] P. S. Kundur and O. P. Malik, *Power System Stability and Control.* New York: McGraw-Hill, 2022, pp. 582-598.
[2] National Nature Science foundation of China. (2022, Jul.). Guidelines for Fundamental Research on the "Dual Carbon" in the National Natural Science Foundation of China. [Online]. Available:https://www.nsfc.gov.cn/publish/portal0/tab442/info86785.htm
[3] P. Babahajiani, Q. Shafiee, and H. Bevrani, "Intelligent demand response contribution in frequency control of multi-area power systems," *IEEE Transactions on Smart Grid*, vol. 9, no. 2, pp. 1282-1291, Mar. 2018.
[4] Z. Xu, J. Ostergaard, and M. Togeby, "Demand as frequency controlled reserve," *IEEE Transactions on Power Systems*, vol. 26, no. 3, pp. 1062-1071, Aug. 2011.
[5] S. Liao, J. Xu, Y. Sun *et al*., "Load-damping characteristic control method in an isolated power system with industrial voltage-sensitive load," *IEEE Transactions on Power Systems*, vol. 31, no. 2, pp. 1118-1128, Mar. 2016.
[6] G. de Carne, G. Buticchi, M. Liserre *et al.*, "Real-time primary frequency regulation using load power control by smart transformers," *IEEE Transactions on Smart Grid*, vol. 10, no. 5, pp. 5630-5639, Sept. 2019.
[7] J. A. Short, D. G. Infield, and L. L. Freris, "Stabilization of grid frequency through dynamic demand control," *IEEE Transactions on Power Systems*, vol. 22, no. 3, pp. 1284-1293, Aug. 2007.
[8] A. Ballanti, L. N. Ochoa, K. Bailey *et al*., "Unlocking new sources of flexibility: CLASS: the world's largest voltage-led load management project," *IEEE Power and Energy Magazine*, vol. 15, no. 3, pp. 52-63, May-Jun. 2017.
[9] S. Y. Hui, C. K. Lee, and F. F. Wu, "Electric springs − a new smart grid technology," *IEEE Transactions on Smart Grid*, vol. 3, no. 3, pp. 1552-1561, Sept. 2012.

[10] Y. Sun, J. Xu, S. Liao *et al*., "Controlled load/frequency response to substantially increase frequency regulation capability for power system with high penetration renewable energy," *Proceedings of the CSEE*, vol. 43, no. 3, pp. 868-877, Feb. 2023.
[11] *Power Quality − Deviation of Supply Voltage*, Chinese Grid Code GB/T 12325-2008, Jun. 2008.
[12] *Technical Rules for Automatic Under-frequency Load Shedding in Electric Power Systems*, Chinese Grid Code GB/T 40596-2021, Oct. 2021.
[13] *Power Quality − Frequency Deviation for Power System*, Chinese Grid Code GB/T 15945-2008, Jun. 2008.
[14] Y. Chen, R. Hesse, D. Turschner *et al*., "Investigation of the virtual synchronous machine in the island mode," in *Proceedings of 2012 3rd IEEE PES Innovative Smart Grid Technologies Europe (ISGT Europe)*, Berlin, Germany, Oct. 2012, pp. 1-6.
[15] L. M. Korunović, J. V. Milanović, S. Z. Djokic *et al*., "Recommended parameter values and ranges of most frequently used static load models," *IEEE Transactions on Power Systems*, vol. 33, no. 6, pp. 5923-5934, Nov. 2018.
[16] A. Cai, Y. Yu, L. Xu *et al*., "Review on reactive power compensation of electric vehicle charging piles," in *Proceedings of 2019 22nd International Conference on Electrical Machines and Systems (ICEMS)*, Harbin, China, Aug. 2019, pp. 1-4.
[17] P. Ju and D. Ma, *Electric Power System Load Modeling*. Beijing: China Electric Power Press, 2008, pp. 153-159.

Zhe Zhang received the B.S. degree in electrical engineering and automation from Wuhan University, Wuhan, China, in 2018. She is currently working toward the Ph.D. degree in electrical engineering and automation from Wuhan University. Her research interests include renewable energy aggregation modeling, load control, and stability and control of energy system with high penetration rate of renewable energy sources.

Siyang Liao received the B.S. and Ph.D. degrees in electrical engineering from Wuhan University, Wuhan, China, in 2011 and 2016, respectively. He is currently an Associated Professor with the School of Electrical Engineering and Automation, Wuhan University. His research interests include wind power integration and power system simulation technology.

Yuanzhang Sun received the Ph.D. degree in electrical engineering from Tsinghua University, Beijing, China, in 1988. He is currently a Professor with the School of Electrical Engineering and Automation, Wuhan University, Wuhan, China, and a Chair Professor with the Department of Electrical Engineering and Vice Director of the State Key Laboratory of Power System Control and Simulation, Tsinghua University. His research interests include power system dynamics and control, voltage stability and control, and reliability.

Jian Xu received the B.S. and Ph.D. degrees in electrical engineering from Wuhan University, Wuhan, China, in 2002 and 2007, respectively. He is currently a Professor with the School of Electrical Engineering and Automation, Wuhan University. His research interests include power system operation, voltage stability, and wind power control and integration.

Deping Ke received the B.S. degree in electrical engineering from Huazhong University of Science and Technology, Wuhan, China, and the Ph.D. degree in electrical engineering from Hong Kong Polytechnic University, Hong Kong, China, in 2005 and 2012, respectively. He is currently an Associate Professor with the School of Electrical Engineering and Automation, Wuhan University, Wuhan, China. His research interests include power system dynamics and control, and economical operation of power systems.

Bo Wang received the B.S. degree in electrical engineering and automation from Wuhan University, Wuhan, China, in 2014, and the M.S. degree in power engineering from Nanyang Technological University, Singapore, in 2015. He is currently working toward the Ph.D. degree with the School of Electrical Engineering and Automation, Wuhan University. His research interests include operation and analysis of power system with renewable energy and load control.

Rui Chen received the B.S. degree in electrical engineering and automation from the Hubei University of Technology, Wuhan, China, in 2016, the M.S. degree in electrical power system engineering from the University of Manchester, Manchester, U.K., in 2017, and the Ph.D. degree in electrical engineering from Wuhan University, Wuhan, China, in 2023. His research interests include power system dynamics and control, wind power, and economic operation of power systems.

Yibo Jiang received the B.S. and Ph.D. degrees in electrical engineering and automation from Hubei University of Technology, Wuhan, China, in 2014 and 2019. He is currently a Researcher at the State Grid (Suzhou) City & Energy Research Institute Company Limited, Suzhou, China. His research interests include coordination and operation methods for integrated energy system, multi-energy flow modeling, and stochastic analysis of renewable energy sources.